Tidal dissipation in rubble-pile asteroids

Francis Nimmo

Department of Earth and Planetary Sciences, University of California Santa Cruz

Isamu Matsuyama

Lunar and Planetary Laboratory, University of Arizona

Abstract

We develop a simple scaling argument for frictional dissipation in rubble-pile asteroids, parameterized as an effective dissipation factor Q. This scaling is combined with a prediction (Goldreich and Sari, 2009) for the tidal response amplitude, parameterized by the Love number k_2. We compare the combined scaling with k_2/Q values inferred from asteroid binaries in which the semi-major axis is determined by a balance between tidal dissipation and the binary YORP (or BYORP) effect (Jacobson and Scheeres, 2011). The k_2/Q scaling matches the inferred values if dissipation is confined to a regolith layer of thickness ∼30 m, similar to the available asteroid regolith thickness estimates. The scaling suggests a regolith thickness that is independent of (or decreases slightly with) increasing asteroid radius; **this result is consistent with at least one model of regolith generation via impacts.**

Keywords:

1. Introduction

The amplitude and phase of an object's response to tides provide information on its internal structure (Moore and Schubert, 2000, e.g.). This response is typically described by the Love numbers k_2 and h_2 (Munk and MacDonald, 1960). **These dimensionless numbers quantify the amplitude of the response to the perturbing tidal potential, where h_2 describes the shape response and k_2 the gravity response. A uniform, strengthless body has h_2=2.5 and k_2=1.5. A body with non-zero rigidity and/or mass concentrated towards its centre will have smaller Love numbers.**

It is often convenient to describe the Love numbers as complex quantities, where the real and imaginary parts describe the in-phase (elastic) and out-of-phase responses (Ross and Schubert, 1989, e.g.). Dissipation only arises if there is a phase lag - a purely elastic response dissipates no energy. Thus, the rate of tidal dissipation depends on $Im(k_2)$. This quantity is sometimes written k_2/Q, where Q is the quality factor and is related to the phase lag of the tidal response (Efroimsky and Makarov, 2013, e.g.). Measurements of the tidal response (real part of k_2) of the Earth, Moon, Venus, Mars and Titan have been used to make deductions about their interiors (Lau et al., 2017; Williams et al., 2014; Konopliv and Yoder, 1996; Yoder et al., 2003; Iess et al., 2012). Such measurements typically require a nearby spacecraft to measure small periodic variations in the body's gravity field.

Tidal dissipation in a body also affects its spin and orbit evolution (Goldreich and Soter, 1966). As a result, under special circumstances the orbital characteristics of a body can be used to infer its tidal response, without requiring a spacecraft. Thus, for instance, measurements of Io's orbital evolution (Lainey et al., 2009) and the orbital characteristics of the exoplanet HAT-P-13b (Batygin et al., 2009) have been used to infer their respective k_2/Q values. Mercury's evolution into a 3:2 spin:orbit resonance (Peale, 1988) and the doubly synchronous Pluto-Charon system (Dobrovolskis et al., 1997) can likewise be used to place bounds on their respective k_2/Q.

Asteroid tidal dissipation is conventionally parameterized either using k_2/Q or $1/\mu Q$, where μ is the rigidity. The use of rigidity μ arises because for a uniform elastic body $k_2 = (3/2)/(1 + \frac{19\mu}{\rho g R})$, where ρ, g and R are the body's density, surface gravity and radius, respectively (Munk and MacDonald, 1960). For a small body, $\mu \gg \rho g R$ and so k_2 scales as $1/\mu$. The relationship between k_2 and rigidity changes if non-elastic effects are included, and is discussed in more detail below (see equation 7). Our approach yields a Q that is frequency-dependent, and thus somewhat resembles the approach of Efroimsky (2015); however, in our model dissipation occurs by granular friction, rather than viscosity. Granular friction has also been suggested as responsible for tidal heating in the silicate core of Enceladus (Choblet et al., 2017).

There are at least three ways of using observations to determine k_2/Q or μQ. The first is to use the present-day semi-major axis of a binary pair (Taylor and Margot, 2011, e.g.). Given an assumed age of the binary **(which**

is usually uncertain), the present-day semi-major axis then yields the approximate μQ of the primary (the uncertainty introduced by the unknown initial semi-major axis is small **as long as the secondary is small**). This approach assumes that tidal dissipation is the only process causing the semi-major axis to expand; if other processes are simultaneously acting to reduce the semi-major axis, this approach only yields an upper bound on μQ.

The second approach instead assumes that the present-day semi-major axis is an equilibrium state, between dissipation in the primary (which expands the semi-major axis) and the so-called binary YORP (or BYORP) effect, which **in the case of a synchronous secondary can cause** the semi-major axis to decrease (Jacobson and Scheeres, 2011). Given the equilibrium semi-major axis and an assumed BYORP strength, the balancing μQ can then be calculated (and will necessarily be smaller - i.e. more dissipative - than using the first approach). Although the YORP effect has been measured directly (Lowry et al., 2007; Taylor et al., 2007), so far the BYORP effect has not. Nonetheless, the semi-major axis drift rate of asteroid (175706) 1996 FG_3 is much less than that expected from tidal effects alone, and is consistent with zero, suggesting that at least in this case an equilibrium situation exists (Scheirich et al., 2015). Last, the existence of tumbling asteroids can be used to derive an approximate value for k_2/Q given an assumed timescale for the excitation of tumbling. Although the excitation timescale is not well-constrained, this approach suggests that μQ decreases with decreasing asteroid size (Pravec et al., 2014).

The main aim of the current paper is to combine the observational constraints on μQ discussed above with a simple model of asteroid dissipation to make inferences about these objects' internal structures. The rest of this paper is organized as follows. In Section 2 we develop a theoretical model for frictional dissipation in small asteroids. In Section 3 we will compare the theory with observational constraints based on the three approaches described above. Based on the example of (175706) 1996 FG_3, we place most reliance on (and spend most time discussing) the second approach, in which BYORP balances tidal dissipation. Finally, in Section 4 we discuss our conclusions, and point out ways in which future spacecraft or Earth-based observations may test our model.

2. Theory

We wish to consider tidal dissipation in a binary rubble-pile asteroid. The external perturbing potential will cause deformation throughout the body, depending on its mechanical properties. We will assume, however, that this deformation results in dissipation only in a **surface** layer of thickness t, which may be less than or equal to the radius of the body R, and which consists of elements of a characteristic size r (Figure 1). The thickness t may be related to the tidal stresses or may be determined by other factors, and will be discussed further below. Dissipation is assumed to take place via sliding friction arising during relative displacement u between neighbouring elements.

We deliberately keep our analysis simple. In particular, because of the large uncertainties associated with the observations, we generally neglect quantities of order unity in the scaling arguments presented below.

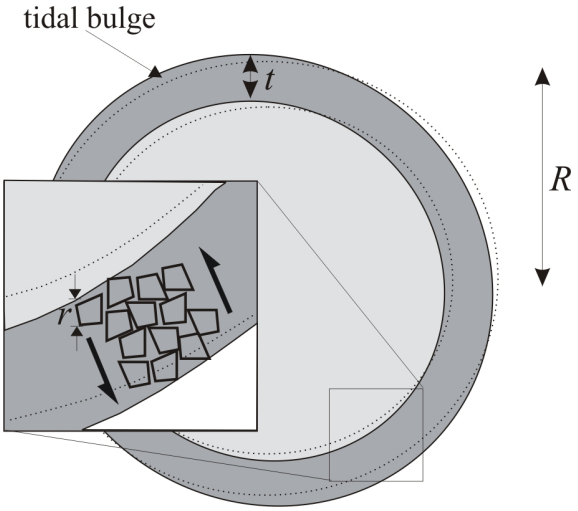

Figure 1 Sketch of the geometry of the problem. Tidal deformation is represented by the departure of the solid surface from the mean shape (dashed lines) and results in shear strains (indicated by half-arrows).

On a single element face, the characteristic dissipation rate $\dot{E}_f$ **is given by the product of shear stress, the sliding velocity and the surface area** and may be written as

$$\dot{E}_f \sim (\rho g t) f r^2 u \Omega_p \tag{1}$$

where u **is the displacement of the element face**, ρ is the density, g the surface gravity, f the friction coefficient during sliding and Ω_p the spin angular frequency of the primary (assumed to be non-synchronous). **The sliding velocity is** $\sim u\Omega_p$**, the surface area is** $\sim r^2$ **and** the quantity in parentheses is the characteristic overburden pressure which is multiplied by the friction coefficient to give the shear stress (Turcotte and Schubert, 2002, e.g.).

Because the primary is assumed to be non-synchronous, the tidal bulge raised on the primary by the secondary will rotate relative to the primary's solid surface. This deformation will cause shear strains in the near-surface layer (Fig 1), producing relative motion and dissipating energy. The characteristic size of the bulge H **is given by (Murray and Dermott, 1999, e.g.)**

$$H = h_2 R \frac{m}{M} \left(\frac{R}{a}\right)^3 \tag{2}$$

where h_2 **is the displacement tidal Love number,** m **and** M **are the mass of the secondary and primary, respectively,** a **is the semi-major axis, and** R **is the primary radius.**

The characteristic displacement u will depend on the element size and the tidal **shear** strain ϵ:

$$u \sim \epsilon r \sim r \left[\frac{H}{R}\right] \sim r h_2 \left[\frac{q}{1+q}\frac{n^2}{G\rho}\right] \tag{3}$$

Here $q = m/M$ is the mass ratio, n is the mean motion (assumed $\ll \Omega_p$) and G is the gravitational constant. The quantity in square brackets is a measure of the tidal acceleration relative to the self-gravity of the primary and will be referred to as the tidal **slope (because it describes the deviation in the surface equipotential due to tides). This quantity can also be written** $(R'/a)^3$**, where** R' **is the radius of the secondary (Goldreich and Sari, 2009).**

The assertion that $u \sim \epsilon r$ **arises as follows. The tidal displacement** H **varies laterally over a lengthscale** $\sim R$**, because it is a degree-2 feature. Thus, the characteristic shear strain is** $\epsilon = H/R$**. The relative radial displacement between two points separated by a horizontal distance** r **will then scale as** ϵr**. If the medium were uniform, this displacement would be distributed evenly; in a granular**

material, the relative displacement will happen between neighbouring element faces but have the same magnitude.

For the asteroids we consider, the typical tidal slope is $\sim 10^{-3}$ (see below). For synchronous satellites, the equivalent diurnal tidal slope is $\sim en^2/G\rho$, where e is the eccentricity, giving a tidal slope $\sim 10^{-5}$ for a tidally-heated moon like Europa. Note, however, that this does not necessarily imply that asteroids are more affected by tides than satellites: the deformation of the body in response to the tidal acceleration depends on h_2 (equation 2), which is larger by a factor of $10^3 - 10^5$ for satellites than for asteroids. Thus, for Europa the diurnal tidal strain ϵ is $\sim 10^{-5}$ while for a typical asteroid it is $\sim 10^{-8}$.

In this approach we are implicitly assuming that the mechanical properties of the body which control its tidal amplitude do not change significantly with depth. This assumption is consistent with the equation we adopt for k_2 (equation 7 below). However, this assumption does not require that the dissipative properties of the body stay constant with depth. In particular, we would expect varying element size to have a much larger effect on tidal dissipation than tidal amplitude. The size of an element will control the relative magnitudes of internal (e.g. viscous) dissipation and external (frictional) dissipation. A large element will undergo differential tidal strain and thus experience more internal dissipation, while a collection of small elements will experience **little internal dissipation and more frictional dissipation**. Since internal dissipation at the relevant temperatures and pressures is essentially zero, large elements will be much less dissipative than small elements. This is consistent with everyday experience - a bag of marbles is much more dissipative than a single giant marble.

The assumption that u scales with the element size (equation 2) is a key part of our argument. This assumption will break down if the elements have sizes of the same order as the **thickness t of the dissipative layer. This assumption can be checked *a posteriori* because some indication of maximum element size can be deduced from observations of boulders at the surface (see Section 4.2)**.

Combining equations 1 and 3, the dissipation rate per **volume** element is independent of r, and the total frictional dissipation rate in the dissipative layer is

$$\dot{E}_f \sim N f h_2 \Omega_p m n^2 t^2 \tag{4}$$

where here N (≈ 3 for a roughly cubic element) is the number of faces per element, divided by two (to avoid double counting) and we have dropped the $(1+q)$ term which is generally $\approx$1. In this expression the t^2 term arises from contributions to the overburden pressure and the volume of dissipative material. Equation 4 shows that the dissipation rate increases with increasing friction coefficient, forcing frequency and displacement (h_2), as expected.

Conventional tidal dissipation in a non-synchronous primary is calculated by (Murray and Dermott, 1999, e.g.)

$$\dot{E} \sim \frac{k_2}{Q} m^2 \frac{R^5}{a^6} G \Omega_p \tag{5}$$

Comparing equations 4 and 5 we can write an *effective* Q for the frictional case, Q_{eff}, as

$$Q_{eff} \sim \left[\frac{qn^2}{G\rho}\right] \frac{1}{Nf} \left(\frac{R}{t}\right)^2 \sim 3 \times 10^{-3} \left(\frac{qn^2}{3 \times 10^{-10}\ s^{-2}}\right) \left(\frac{2\ g/cc}{\rho}\right) \left(\frac{R}{t}\right)^2 \tag{6}$$

where here we have assumed that $h_2 \approx k_2$, as appropriate for **an order of magnitude argument**. We take the bulk density ρ to be 2 g/cc; the static friction factor for silicates is about 0.6, so we take the quantity Nf to be of order unity. The body becomes more dissipative (lower Q) with higher friction or a thicker dissipative layer, as expected. However, the effective Q increases (less dissipation) with increasing tidal **slope**. This is a consequence of the fact that conventional tidal dissipation (equation 5) is more sensitive to tidal **slope** than is frictional dissipation. Since we will make use below of results assuming conventional dissipation, the functional form of Q_{eff} is important. We also note that, so far, we are not assuming any particular functional form for t.

3. Comparison with Observations

The two most relevant sets of observational constraints are the analyses of asteroid binary pairs carried out by Jacobson and Scheeres (2011) and Taylor and Margot (2011). An important theoretical paper is that by Goldreich and Sari (2009), in which the k_2 tidal response of a rubble-pile asteroid is calculated assuming that stress concentrations and plastic yielding are important.

Goldreich and Sari predict that the tidal response of a rubble-pile asteroid is given by

$$k_2 \sim \rho R \left(\frac{G\epsilon_Y}{\mu} \right)^{1/2} \sim 10^{-8} R \tag{7}$$

where here μ is the shear modulus of unfractured rock, ϵ_Y is the yield strain and here and in later equations numerical constants are given assuming quantities are expressed in SI units. Larger asteroids are subject to more yielding because the overburden pressure is higher, and thus develop larger values of k_2.

3.1. Jacobson and Scheeres (2011)

Jacobson and Scheeres (2011) (hereafter JS11) assumed a balance between BYORP and tides to calculate BQ/k_2 **for binaries with synchronous secondaries**. Here B is a parameter describing the strength of the BYORP effect which depends on asteroid shape, but is assumed to be independent of radius. **We updated their calculations using an expanded data set of binaries with synchronous secondaries, using Pravec et al. (2016), and tabulate the results in Table 1. There are small differences to the JS11 calculations, mostly arising from updated radius values.** The results are plotted in Fig 2a below, and demonstrate (as JS11 note) that BQ/k_2 scales approximately linearly with radius. The formal least-squares regression (dashed line) has a slope of **1.51**, but for the majority of this paper we will follow JS11 and assume that $BQ/k_2 \sim R$; **we discuss this issue further in Section 4.2.**

As JS11 point out, if Q and B are constant, then the dependence seen in Fig 2a is different by a factor of R^2 to the Goldreich and Sari prediction (equation 7). In this context, equation 6 is of immediate interest, because it suggests that, if t is constant, Q should scale as R^2 and so BQ/k_2 should scale as R, as observed. Equation 6 further predicts that Q will scale as the tidal **slope**, $qn^2/G\rho$, which can also be compared with observations (see below).

Although JS11 took $B \approx 10^{-3}$, Scheirich et al. (2015) point out that this was an error and that a more likely value is $B \approx 10^{-2}$. The observations of JS11 can thus be written

$$\frac{Q}{k_2} \sim 3 \times 10^2 R \tag{8}$$

Using equation 8 and substituting in the Goldreich and Sari prediction (equation 7) we have

$$Q \sim 3 \times 10^{-6} R^2 \tag{9}$$

Equation (9) yields the same result as the prediction of (6) if t is independent of radius. For the asteroids examined by JS11 typical values are $n \sim 10^{-4} s^{-1}$ and $q \sim 0.03$; with these parameters, equation (6) then yields $t \sim 30$ m. **If instead we took** $BQ/k_2 \sim R^{3/2}$ **we would instead obtain** $t \sim 30$ m$(R/1$ km$)^{-1/4}$**.**

For completeness, with k_2 given by Goldreich and Sari (equation 7) and Q given by equation 6 we have

$$\frac{Q}{k_2} \sim 3 \times 10^5 \left(\frac{R}{1\ km}\right) \left(\frac{qn^2}{3 \times 10^{-10}\ s^{-2}}\right) \left(\frac{2\ g/cc}{\rho}\right) \left(\frac{30\ m}{t}\right)^2 \tag{10}$$

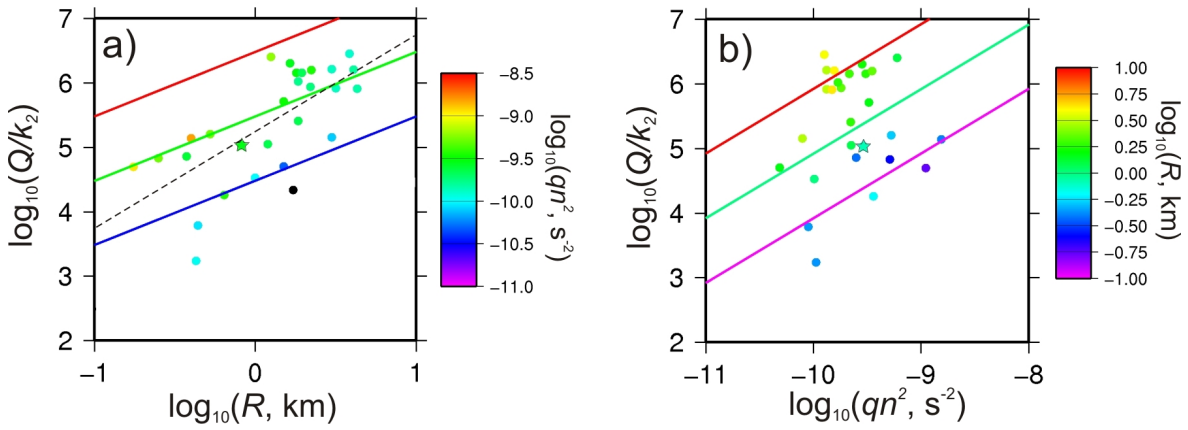

Figure 2 a) Dots are data plotted from Table 1 taking $B = 10^{-2}$ (see text); colour indicates tidal **slope** (qn^2). Star is (175706) 1996 FG_3 (Scheirich et al. 2015). Dashed line shows least-squares fit to the data, with a gradient of **1.51**. Coloured lines use equation 10 with three different values of tidal **slope** ($10^{-8.5}, 10^{-9.5}, 10^{-10.5}$ s^{-2}) and t=30 m. b) As for a) but plotting data against qn^2. Lines assume three different values of R (0.1, 1, 10 km) and t=30 m.

Figure 2a plots the data from Table 1, with each asteroid colour-coded according to the tidal **slope**. It is apparent that, for a given radius, bodies with larger inferred values of Q/k_2 tend to be those experiencing larger tidal **slope**s, as expected from equation 10. The coloured lines in Fig 2a use

equation (10) with three different values of tidal **slope** and t=30 m. Although the data are scattered, the model captures the sensitivity to R and qn^2 **reasonably well**. Figure 2b is similar to 2a but now plots the variation in Q/k_2 as a function of qn^2. For the same tidal **slope** larger asteroids are less dissipative. Again, the spread in the data is approximately consistent with the theoretical model, **although an $R^{3/2}$ dependence would improve the fit**.

3.2. Taylor and Margot (2011)

We may also compare our calculation results with the inferred μQ obtained by Taylor and Margot (2011), hereafter TM11. As noted above, since these inferred values neglect BYORP, they are likely to provide upper bounds. For small bodies the relationship of μ to k_2 is $\mu \sim \rho^2 R^2 G/k_2$ (Goldreich and Sari, 2009). Using equation (10) we thus derive

$$\mu Q \sim 10^8 \left(\frac{R}{1\ km}\right)^3 \left(\frac{qn^2}{3\times 10^{-10}}\right) \left(\frac{30\ m}{t}\right)^2 \tag{11}$$

This prediction may be compared directly with the μQ values derived by TM11. Figure 3 plots the calculated μQ using equation 11 with t = 3 m against the measured μQ. The general trends seen in both Figs 3a and 3b are reproduced reasonably well by the model. This approach results in less dissipative asteroids than for Fig 2 (as expected), which in our model results in a thinner dissipative layer (lower t). We note that the asteroids shown in Fig 2 represent a subset of the asteroids used by TM11 (Fig 3). There is thus a set of asteroids for which we have two estimates of the dissipative properties.

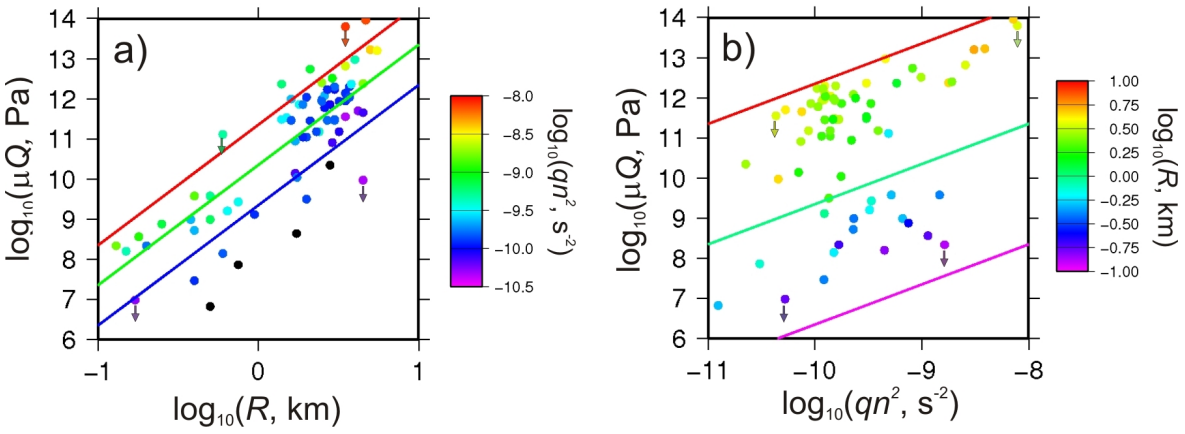

Figure 3 a) As for Fig 2a, but using the data of Taylor and Margot (their Tables 2 and 3) and comparing with the prediction of equation 11. Here t=3 m **(rather than 30 m in Fig 2)**. b) As for Fig 2b, but with t=3 m. Arrows on some data points are to remind the reader that all estimated values are upper limits (see text).

The results of Scheirich et al. (2015) for (175706) 1996 FG_3 are thus of considerable importance. TM11's analysis yields a μQ of 2.7×10^9 Pa for this body. As noted above, the absence of any detected semi-major axis drift for this body strongly suggests an equilibrium state in which BYORP and tides balance (the JS11 assumption), and in this case $\mu Q \approx 8.2 \times 10^6$. For a body with 1996 FG_3's parameter values (q=0.025, R=0.82 km, ρ=1.3 g/cc and $n = 1.07 \times 10^{-4}$ s^{-1}), equation 11 shows that $t \approx$76 m. This is broadly consistent with the estimates of t derived from the JS11 analysis (Section 3.1). Based on this example we place more weight on the JS11 results than the TM11 results, but point out that future observations of other asteroids are required to provide confirmation of the equilibrium semi-major axis hypothesis.

3.3. Pravec et al. (2014)

Pravec et al. (2014) show that the line dividing tumbling from non-tumbling asteroids yields a damping timescale which is approximately independent of radius. Since the excitation timescale for tumbling is expected to be radius-dependent, one would expect the damping timescale to also depend on radius. These authors suggest that their result may be due to the fact that μQ, which controls the damping timescale, is itself radius-dependent. The equations given in Pravec et al. (2014) show that for the damping timescale

to remain constant, μQ would need to scale as R^2. Our equation (11) predicts that, for a constant t, μQ instead goes as R^3. Thus, while our results provide qualitative agreement with the Pravec et al. (2014), there is not quantitative agreement.

4. Discussion

The analysis above suggests that the JS11 observational constraints can be satisfied by frictional dissipation if two conditions are met: the thickness of the layer in which dissipation occurs (t) is independent of (or decreases slightly with) R; and the thickness of this layer is of order 30 m. The question is whether either of these conditions is reasonable.

4.1. Regolith thickness

The simplest way to explain the dissipative layer is to appeal to a granular layer (a regolith) that is ∼30 m thick, with less disrupted, more monolithic and less dissipative material beneath. Such a situation resembles the near-surface structure of the Moon, in which the near-surface consists of fine-grained material, while at greater depths larger, fractured blocks are present (Heiken et al., 1991, Fig 4.22). Observational constraints on asteroid regolith thicknesses are scanty. On Itokawa (mean R=0.17 km), the regolith thickness is a few metres or more deep, at least locally (Barnouin-Jha et al., 2008). Grooves on Gaspra (R=6.1 km) might suggest a regolith layer of thickness 30-200 m (Veverka et al., 1994), although this is uncertain. On Eros (R=8.4 km), groove dimensions have been used to suggest a regolith thickness of up to a few tens of metres (Prockter et al., 2002). Thomas et al. (1979) concluded that grooves on Phobos (R=11.3 km) suggested a regolith thickness of 100-200 m. On Ida (R=15.7 km), weak, mobile surface materials are estimated to extend to a depth of ∼50 m (Sullivan et al., 1996).

Based on the summary above, a regolith thickness of order 30 m would be hard to rule out, except perhaps for Itokawa. As far as the dependence of t on R goes, Itokawa is two orders of magnitude smaller than Ida, yet the inferred regolith is only an order of magnitude thinner. At the very least, this suggests that the linear dependence of t on R sometimes assumed (Haack et al., 1990, e.g.) is too strong (see below).

In terms of mechanisms, one might expect an impact-dominated regolith thickness to scale in some fashion with radius. However, even the sign of the scaling is unclear (Haack et al., 1990,

e.g.). Housen et al. (1979) argue that regolith thickness increases markedly with increasing radius, while Langevin and Maurette (1980) argue that for small asteroids the expected regolith thickness is tens of metres, and decreases slightly with radius. The latter's conclusions are thus fully consistent with our findings.

Another complicating factor may be the role of thermal fatigue as a regolith-generating process (Delbo et al., 2014). This process will not directly depend on body size. However, the thermal skin depth is too shallow for thermal stresses to be directly generating regolith at decameter depths. At a minimum, some other mechanism must be circulating material from these depths to the surface, for instance impact gardening or perhaps shaking-induced convection (Yamada et al., 2016).

Rather than appealing to a regolith thickness determined by other processes, there might instead only be a regolith sub-layer (of thickness ∼30 m) in which significant dissipation occurs. One could imagine that at some critical depth the frictional stress arising from the overburden pressure exceeds the tidal shear stresses causing relative motion. Such a thin, surficial mobile sub-layer is a common outcome in granular flow experiments (Allen and Kudrolli, 2017, e.g.). Furthermore, since surface boulders rarely exceed 10 m in diameter (Chapman et al., 2002; Michikami et al., 2008, e.g.), the inferred sub-layer thickness might be as small as only a few "grains" thick, consistent with the experiments.

Using Goldreich and Sari (2009), the tidal stress (force per unit area at the primary surface) is $(mg/R^2)(R/a)^3 \sim (qn^2/G)Rg$, where g is the surface gravity and m is the mass of the secondary. If grains cannot move past each other, then the near-surface regolith will act as a monolithic layer, resembling the shell of an icy satellite. In such a case, the tidal stresses can be compared with the overburden pressure to calculate the depth to which fractures could open (Smith-Konter and Pappalardo, 2008, e.g.). In this case, given an overburden stress of $\rho g z$, the depth to which fractures could open is $z \sim [qn^2/\rho G]R = [(R'/a)^3]R$. Here the quantity in brackets is the tidal slope and for our nominal parameters we obtain a depth of a few meters. Note that we are neglecting the role of any cohesive forces, which may not be entirely negligible in such a low-stress environment (Scheeres and Sánchez, 2018). This caveat aside, at least in the very near-surface it appears that grains can move past

each other under the influence of tidal stresses, although we concur with GS09 that in the bulk of the asteroid such relative motion is not possible ("cracks don't matter"). More to the point, however, if we assume that the thickness t is controlled by the fracture-opening depth, then the predicted linear dependence of t on R is not consistent with our results, so we do not pursue this line of argument further.

4.2. Regolith thickness - radius scaling

So far we have argued, based on a linear $Q/k_2 - R$ relationship that the regolith thickness t should be independent of body radius R. However, if one takes equation (10) and uses the measured Q/k_2 values to derive t, the derived t actually decreases somewhat with increasing radius (Table 1). The range in derived t-values for data is quite small (12 to 191 m), and overlaps with the estimated thicknesses enumerated above, but nonetheless this is a surprising result. The likely explanation is that Q/k_2 actually varies more like $R^{3/2}$ (Fig 2a) and, as a result, equation (10) implies t must scale as $R^{-1/4}$. **This dependence would also improve the fit to the observations plotted in Fig 2b.** In any event, it implies that if anything, regolith thickness should decrease with increasing radius.

4.3. Asteroid mechanical properties

In our approach we assume that the amplitude of the tidal response of a rubble-pile asteroid is determined by its bulk interior material properties, such as shear modulus and yield strain (equation 7). The rate of dissipation, however, **will depend strongly on whether the material is monolithic blocks or fine-grained regolith (Section 2).** We hypothesize that the dissipated energy budget is dominated by the near-surface regolith. This picture is in contrast to the idea proposed by Hurford et al. (2016), in which the tidal amplitude of Phobos is hypothesized to be controlled by a rigid surface layer (the regolith) overlying a weak interior.

The situation we envisage is somewhat reminiscent of the situation on Earth, where the overall tidal amplitude is controlled by the bulk material properties of the interior, while the dissipation is dominated by a thin surficial layer (the ocean). **An important difference is that water, having no shear strength, will flow laterally in response to the small tidal slopes ($\sim 10^{-7}$) imposed by the lunar tides. A rocky regolith layer will not flow laterally in this way, because static friction vastly**

exceeds the small tidal slopes; however, the tidal displacement of the underlying material will still cause shear strains in the layer, and thus dissipation (Figure 1).

4.4. Long-term binary evolution

If equation (10) is correct, then the long-term orbital evolution of the binary system will require modification, because Q/k_2 is now frequency-dependent rather than being constant, as is usually assumed. However, the only effect on the usual tidal evolution equations (Murray and Dermott, 1999, e.g.) is to introduce an additional constant factor of order unity. As a result, the long-term evolution will be qualitatively the same as for a constant-Q case.

5. Conclusions

It currently appears that the most parsimonious explanation of the JS11 observations is that asteroids possess a dissipative regolith layer a few decameters thick, independent of (or even decreasing slightly with) body radius. Beneath the regolith layer is a more monolithic, although still fractured, interior which is much less dissipative, but which nonetheless controls the overall amplitude of the tidal response. **Encouragingly, our regolith thickness estimates are consistent with the asteroid-regolith generation model developed by Langevin and Maurette (1980).**

We can envisage at least **three** pathways forwards. The first is to carry out numerical experiments on frictional dissipation in tidally-perturbed asteroids, ideally including polyhedral fragments in a manner similar to Movshovitz et al. (2012). **These results may then be compared with our simple scaling arguments**. **A second is to investigate whether the model of Langevin and Maurette (1980) still holds, in view of more recent developments in modeling of impact processes and regolith redistribution (Korycansky and Asphaug, 2004, e.g.).** The third is to test our analysis with upcoming observations. For instance, astrometry (as demonstrated by Scheirich et al. (2015)) can potentially be used to measure k_2/Q and thus predict the regolith thickness via equation (10). Remote sensing observations (e.g. radar sounding, detailed gravity mapping or morphometric analysis by future spacecraft such as OSIRIS-REx) will then allow measurement of regolith thickness and comparison with the predictions.

Acknowledgements We thank two reviewers for their insightful reading of the original MS.

Table 1 Binary asteroids with synchronous secondaries using the 2015-09-18 update from http://www.asu.cas.cz/∼asteroid/binastdata.htm (see Pravec et al. (2016)). Entries in bold were also used in JS11; of the remainder, entries in italics are for systems where the synchronous rotation of the secondary is uncertain. Here a_h and e_h are the heliocentric semi-major axis and eccentricity; ρ is assumed to be 2 g/cc in the absence of other information; and BQ/k_2 is calculated using the same approach as in JS11, taking the solar radiation constant to be 4.4×10^{-6} kg m^{-1} s^{-2} (McMahon and Scheeres, 2010). The final column is the predicted regolith thickness t calculated using the observations and equation (10) with $B = 10^{-2}$.

Name	a_h AU	e_h	ρ g/cc	q	R_p km	$a(R_p)$	BQ/k_2	t m
(1338) Duponta	2.264	0.112	2	0.0128	3.85	3.86	28400	12
(1453) Fennia	1.897	0.029	2	0.0230	3.17	4.63	8240	21
(2044) Wirt	2.380	0.344	2	0.0156	3.0	4.06	16400	15
(2121) Sevastopol	2.183	0.179	2	0.0674	4.30	6.46	8040	27
(2131) Mayall	1.887	0.111	2	0.0283	4.10	4.70	16100	19
(3309) Brorfelde	1.817	0.053	2	0.0203	2.20	3.99	8670	20
(5407) 1992 AX	1.838	0.278	2	0.0101	1.85	3.23	10500	16
(5477) Holmes	1.917	0.076	2	0.0640	1.50	4.88	5110	29
(5481) Kiuchi	2.339	0.063	2	0.0439	1.80	4.37	14300	19
(5905) Johnson	1.910	0.072	2	0.0546	2.24	4.51	15900	21
(6084) Bascom	2.313	0.236	2	0.0493	3.0	7.14	1420	39
(7088) Ishtar	1.981	0.390	2	0.0736	0.53	4.38	1600	39
(8306) Shoko	2.242	0.220	2	0.0963	1.20	6.41	1120	46
(9260) Edwardolson	2.290	0.229	2	0.0224	1.95	3.90	14300	16
(17260) 2000 JQ58	2.205	0.184	2	0.0203	1.65	3.44	20200	14
(44620) 1999 RS43	2.176	0.165	2	0.0376	1.0	5.99	338	52
(65803) Didymos	1.644	0.38	2	0.0116	0.380	2.98	718	34
(66063) 1998 RO1	0.991	0.720	2	0.1072	0.40	3.50	1370	64
(66391) 1999 KW4	0.642	0.688	2	0.0361	0.64	3.86	181	107
(76818) 2000 RG79	1.930	0.096	2	0.0393	1.25	3.36	25400	16
(80218) 1999 VO123	2.219	0.027	2	0.0322	0.44	5.92	61	76
(85938) 1999 DJ4	1.852	0.484	2	0.1150	0.18	4.00	493	59
(137170) 1999 HF1	0.819	0.463	2	0.0144	1.85	3.32	2560	38
(175706) 1996 FG3	1.054	0.349	1.3	0.0251	0.82	3.17	1080	55
(185851) 2000 DP107	1.366	0.377	1.3	0.0618	0.43	6.08	17	191
(276049) 2002 CE26	2.233	0.560	0.8	0.0007	1.73	2.61	216	38
(285263) 1998 QE2	2.423	0.572	0.7	0.0156	1.50	4.00	507	61
(399774) 2005 NB7	2.044	0.518	2	0.0393	0.25	3.55	679	41

References

Allen, B., Kudrolli, A., Feb. 2017. Depth resolved granular transport driven by shearing fluid flow. Physical Review Fluids 2 (2), 024304.

Barnouin-Jha, O. S., Cheng, A. F., Mukai, T., Abe, S., Hirata, N., Nakamura, R., Gaskell, R. W., Saito, J., Clark, B. E., Nov. 2008. Small-scale topography of 25143 Itokawa from the Hayabusa laser altimeter. Icarus 198, 108–124.

Batygin, K., Bodenheimer, P., Laughlin, G., Oct. 2009. Determination of the Interior Structure of Transiting Planets in Multiple-Planet Systems. Astrophys. J. Lett. 704, L49–L53.

Chapman, C. R., Merline, W. J., Thomas, P. C., Joseph, J., Cheng, A. F., Izenberg, N., Jan. 2002. Impact History of Eros: Craters and Boulders. Icarus 155, 104–118.

Choblet, G., Tobie, G., Sotin, C., Běhounková, M., Čadek, O., Postberg, F., Souček, O., Nov. 2017. Powering prolonged hydrothermal activity inside Enceladus. Nature Astronomy 1, 841–847.

Delbo, M., Libourel, G., Wilkerson, J., Murdoch, N., Michel, P., Ramesh, K. T., Ganino, C., Verati, C., Marchi, S., Apr. 2014. Thermal fatigue as the origin of regolith on small asteroids. Nature 508, 233–236.

Dobrovolskis, A. R., Peale, S. J., Harris, A. W., 1997. Dynamics of the Pluto-Charon Binary. p. 159.

Efroimsky, M., Oct. 2015. Tidal Evolution of Asteroidal Binaries. Ruled by Viscosity. Ignorant of Rigidity. Astron. J. 150, 98.

Efroimsky, M., Makarov, V. V., Feb. 2013. Tidal Friction and Tidal Lagging. Applicability Limitations of a Popular Formula for the Tidal Torque. Astrophys. J. 764, 26.

Goldreich, P., Sari, R., Jan. 2009. Tidal Evolution of Rubble Piles. Astrophys. J. 691, 54–60.

Goldreich, P., Soter, S., 1966. Q in the Solar System. Icarus 5, 375–389.

Haack, H., Rasmussen, K. L., Warren, P. H., Apr. 1990. Effects of regolith/megaregolith insulation on the cooling histories of differentiated asteroids. J. Geophys. Res. 95, 5111–5124.

Heiken, G. H., Vaniman, D. T., French, B. M., 1991. Lunar sourcebook - A user's guide to the moon.

Housen, K. R., Wilkening, L. L., Chapman, C. R., Greenberg, R., Sep. 1979. Asteroidal regoliths. Icarus 39, 317–351.

Hurford, T. A., Asphaug, E., Spitale, J. N., Hemingway, D., Rhoden, A. R., Henning, W. G., Bills, B. G., Kattenhorn, S. A., Walker, M., Jun. 2016. Tidal disruption of Phobos as the cause of surface fractures. Journal of Geophysical Research (Planets) 121, 1054–1065.

Iess, L., Jacobson, R. A., Ducci, M., Stevenson, D. J., Lunine, J. I., Armstrong, J. W., Asmar, S. W., Racioppa, P., Rappaport, N. J., Tortora, P., Jul. 2012. The Tides of Titan. Science 337, 457.

Jacobson, S. A., Scheeres, D. J., Jul. 2011. Long-term Stable Equilibria for Synchronous Binary Asteroids. Astrophys. J. Lett. 736, L19.

Konopliv, A. S., Yoder, C. F., 1996. Venusian k $_2$ tidal Love number from Magellan and PVO tracking data. Geophys. Res. Lett. 23, 1857–1860.

Korycansky, D. G., Asphaug, E., Sep. 2004. Simulations of impact ejecta and regolith accumulation on Asteroid Eros. Icarus 171, 110–119.

Lainey, V., Arlot, J.-E., Karatekin, Ö., van Hoolst, T., Jun. 2009. Strong tidal dissipation in Io and Jupiter from astrometric observations. Nature 459, 957–959.

Langevin, Y., Maurette, M., Mar. 1980. A Model for Small Body Regolith Evolution: the Critical Paramters. In: Lunar and Planetary Science Conference. Vol. 11 of Lunar and Planetary Science Conference. pp. 602–604.

Lau, H. C. P., Mitrovica, J. X., Davis, J. L., Tromp, J., Yang, H.-Y., Al-Attar, D., Nov. 2017. Tidal tomography constrains Earth's deep-mantle buoyancy. Nature 551, 321–326.

Lowry, S. C., Fitzsimmons, A., Pravec, P., Vokrouhlický, D., Boehnhardt, H., Taylor, P. A., Margot, J.-L., Galád, A., Irwin, M., Irwin, J., Kusnirák, P., Apr. 2007. Direct Detection of the Asteroidal YORP Effect. Science 316, 272.

McMahon, J., Scheeres, D., Mar. 2010. Secular orbit variation due to solar radiation effects: a detailed model for BYORP. Celestial Mechanics and Dynamical Astronomy 106, 261–300.

Michikami, T., Nakamura, A. M., Hirata, N., Gaskell, R. W., Nakamura, R., Honda, T., Honda, C., Hiraoka, K., Saito, J., Demura, H., Ishiguro, M., Miyamoto, H., Jan. 2008. Size-frequency statistics of boulders on global surface of asteroid 25143 Itokawa. Earth, Planets, and Space 60, 13–20.

Moore, W. B., Schubert, G., Sep. 2000. NOTE: The Tidal Response of Europa. Icarus 147, 317–319.

Movshovitz, N., Asphaug, E., Korycansky, D., Nov. 2012. Numerical Modeling of the Disruption of Comet D/1993 F2 Shoemaker-Levy 9 Representing the Progenitor by a Gravitationally Bound Assemblage of Randomly Shaped Polyhedra. Astrophys. J. 759, 93.

Munk, W. H., MacDonald, G. J. F., 1960. The rotation of the earth; a geophysical discussion.

Murray, C. D., Dermott, S. F., 1999. Solar system dynamics.

Peale, S. J., 1988. The rotational dynamics of Mercury and the state of its core. pp. 461–493.

Pravec, P., Scheirich, P., Kušnirák, P., Hornoch, K., Galád, A., Naidu, S. P., Pray, D. P., Világi, J., Gajdoš, Š., Kornoš, L., Krugly, Y. N., Cooney, W. R., Gross, J., Terrell, D., Gaftonyuk, N., Pollock, J., Husárik, M., Chiorny, V., Stephens, R. D., Durkee, R., Reddy, V., Dyvig, R., Vraštil, J., Žižka, J., Mottola, S., Hellmich, S., Oey, J., Benishek, V., Kryszczyńska, A., Higgins, D., Ries, J., Marchis, F., Baek, M., Macomber, B., Inasaridze, R., Kvaratskhelia, O., Ayvazian, V., Rumyantsev, V., Masi, G., Colas, F., Lecacheux, J., Montaigut, R., Leroy, A., Brown, P., Krzeminski, Z., Molotov, I., Reichart, D., Haislip, J., LaCluyze, A., Mar. 2016. Binary asteroid population. 3. Secondary rotations and elongations. Icarus 267, 267–295.

Pravec, P., Scheirich, P., Ďurech, J., Pollock, J., Kušnirák, P., Hornoch, K., Galád, A., Vokrouhlický, D., Harris, A. W., Jehin, E., Manfroid, J., Opitom, C., Gillon, M., Colas, F., Oey, J., Vraštil, J., Reichart, D., Ivarsen, K., Haislip, J., LaCluyze, A., May 2014. The tumbling spin state of (99942) Apophis. Icarus 233, 48–60.

Prockter, L., Thomas, P., Robinson, M., Joseph, J., Milne, A., Bussey, B., Veverka, J., Cheng, A., Jan. 2002. Surface Expressions of Structural Features on Eros. Icarus 155, 75–93.

Ross, M. N., Schubert, G., Mar. 1989. Viscoelastic models of tidal heating in Encedalus. Icarus 78, 90–101.

Scheeres, D. J., Sánchez, P., Dec. 2018. Implications of cohesive strength in asteroid interiors and surfaces and its measurement. Progress in Earth and Planetary Science 5, 25.

Scheirich, P., Pravec, P., Jacobson, S. A., Ďurech, J., Kušnirák, P., Hornoch, K., Mottola, S., Mommert, M., Hellmich, S., Pray, D., Polishook, D., Krugly, Y. N., Inasaridze, R. Y., Kvaratskhelia, O. I., Ayvazian, V., Slyusarev, I., Pittichová, J., Jehin, E., Manfroid, J., Gillon, M., Galád, A., Pollock, J., Licandro, J., Alí-Lagoa, V., Brinsfield, J., Molotov, I. E., Jan. 2015. The binary near-Earth Asteroid (175706) 1996 FG_3 - An observational constraint on its orbital evolution. Icarus 245, 56–63.

Smith-Konter, B., Pappalardo, R. T., Dec. 2008. Tidally driven stress accumulation and shear failure of Enceladus's tiger stripes. Icarus 198, 435–451.

Sullivan, R., Greeley, R., Pappalardo, R., Asphaug, E., Moore, J. M., Morrison, D., Belton, M. J. S., Carr, M., Chapman, C. R., Geissler, P., Greenberg, R., Granahan, J., Head, III, J. W., Kirk, R., McEwen, A., Lee, P., Thomas, P. C., Veverka, J., Mar. 1996. Geology of 243 Ida. Icarus 120, 119–139.

Taylor, P. A., Margot, J.-L., Apr. 2011. Binary asteroid systems: Tidal end states and estimates of material properties. Icarus 212, 661–676.

Taylor, P. A., Margot, J.-L., Vokrouhlický, D., Scheeres, D. J., Pravec, P., Lowry, S. C., Fitzsimmons, A., Nolan, M. C., Ostro, S. J., Benner, L. A. M., Giorgini, J. D., Magri, C., Apr. 2007. Spin Rate of Asteroid (54509) 2000 PH5 Increasing Due to the YORP Effect. Science 316, 274.

Thomas, P., Veverka, J., Bloom, A., Duxbury, T., Dec. 1979. Grooves on PHOBOS - Their distribution, morphology and possible origin. J. Geophys. Res. 84, 8457–8477.

Turcotte, D. L., Schubert, G., Apr. 2002. Geodynamics - 2nd Edition.

Veverka, J., Thomas, P., Simonelli, D., Belton, M. J. S., Carr, M., Chapman, C., Davies, M. E., Greeley, R., Greenberg, R., Head, III, J., Klaasen, K., Johnson, T. V., Morrison, D., Neukum, G., Jan. 1994. Discovery of grooves on Gaspra. Icarus 107, 72.

Williams, J. G., Konopliv, A. S., Boggs, D. H., Park, R. S., Yuan, D.-N., Lemoine, F. G., Goossens, S., Mazarico, E., Nimmo, F., Weber, R. C., Asmar, S. W., Melosh, H. J., Neumann, G. A., Phillips, R. J., Smith, D. E., Solomon, S. C., Watkins, M. M., Wieczorek, M. A., Andrews-Hanna, J. C., Head, J. W., Kiefer, W. S., Matsuyama, I., McGovern, P. J., Taylor, G. J., Zuber, M. T., Jul. 2014. Lunar interior properties from the GRAIL mission. Journal of Geophysical Research (Planets) 119, 1546–1578.

Yamada, T. M., Ando, K., Morota, T., Katsuragi, H., Jul. 2016. Timescale of asteroid resurfacing by regolith convection resulting from the impact-induced global seismic shaking. Icarus 272, 165–177.

Yoder, C. F., Konopliv, A. S., Yuan, D. N., Standish, E. M., Folkner, W. M., Apr. 2003. Fluid Core Size of Mars from Detection of the Solar Tide. Science 300, 299–303.